Cerebral Cortex July 2015;25:1782–1791
doi:10.1093/cercor/bht417
Advance Access publication January 14, 2014

Differential Receptive Field Properties of Parvalbumin and Somatostatin Inhibitory Neurons in Mouse Auditory Cortex

Ling-yun Li[1,4], Xiaorui R. Xiong[1,4], Leena A. Ibrahim[1,4], Wei Yuan[1,5], Huizhong W. Tao[1,3] and Li I. Zhang[1,2]

[1]Zilkha Neurogenetic Institute, [2]Department of Physiology and Biophysics, [3]Department of Cell and Neurobiology, [4]Neuroscience Graduate Program, Keck School of Medicine, University of Southern California, Los Angeles, CA 90089, USA and [5]Department of Otolaryngology of Southwest Hospital, Third Military Medical University, Chongqing 400038, China

Address correspondence to Email: liizhang@usc.edu (L.I.Z.) and weiyan175@sina.com (W.Y.)

Cortical inhibitory circuits play important roles in shaping sensory processing. In auditory cortex, however, functional properties of genetically identified inhibitory neurons are poorly characterized. By two-photon imaging-guided recordings, we specifically targeted 2 major types of cortical inhibitory neuron, parvalbumin (PV) and somatostatin (SOM) expressing neurons, in superficial layers of mouse auditory cortex. We found that PV cells exhibited broader tonal receptive fields with lower intensity thresholds and stronger tone-evoked spike responses compared with SOM neurons. The latter exhibited similar frequency selectivity as excitatory neurons. The broader/weaker frequency tuning of PV neurons was attributed to a broader range of synaptic inputs and stronger subthreshold responses elicited, which resulted in a higher efficiency in the conversion of input to output. In addition, onsets of both the input and spike responses of SOM neurons were significantly delayed compared with PV and excitatory cells. Our results suggest that PV and SOM neurons engage in auditory cortical circuits in different manners: while PV neurons may provide broadly tuned feedforward inhibition for a rapid control of ascending inputs to excitatory neurons, the delayed and more selective inhibition from SOM neurons may provide a specific modulation of feedback inputs on their distal dendrites.

Keywords: auditory cortex, inhibitory subtype, interneuron, in vivo patch recording, two-photon imaging, whole-cell recording

Introduction

In the auditory cortex, inhibitory circuits play important roles in the processing of acoustic information. For example, they define the spectral and intensity tuning, shape the temporal aspects of sound-evoked responses and contribute to binaural hearing (Wehr and Zador 2003; Zhang et al. 2003; Tan et al. 2004, 2007; Wu et al. 2006; Razak and Fuzessery 2010; Sadagopan and Wang 2010; Zhou et al. 2012). This inhibitory control is mediated by GABAergic interneurons through feedforward or feedback connections (Callaway 1998; Douglas and Martin 2004; Wu et al. 2011). The inhibitory neurons, comprising only a small fraction of cortical cell population, belong to dozens of morphologically and neurochemically distinct groups (Kawaguchi and Kubota 1997; Markram et al. 2004). Despite the functional importance of inhibitory neurons in auditory cortical processing, little is known about the functional properties of these neurons of diverse types, due to the difficulty of identifying these neurons in vivo. Previously, fast-spiking putative inhibitory units have been isolated based on their narrow spike waveforms. These units differ from regular-spiking (putative excitatory) units at some aspects of response and receptive field properties. For example, fast-spiking units have broader spectral tuning and shorter response latencies compared with regular-spiking cells (Atencio and Schreiner 2008; Wu et al. 2008). However, the spike-waveform-based identification of putative inhibitory neurons is imperfect (Andermann et al. 2004; Barthó et al. 2004). Some pyramidal cells may also have short-duration action potentials that may create classification errors (Gray and McCormick 1996). This issue was further complicated by a recent study (Moore and Wehr 2013) showing that parvalbumin (PV) inhibitory neurons, which are commonly thought to correspond to fast-spiking units, and pyramidal neurons have much larger overlapping distributions of spike-waveform parameters than previously indicated. Intracellular recordings with combined morphological reconstruction and cytochemical analysis are thus required for a full identification. Furthermore, other nonfast-spiking inhibitory neurons cannot be identified in a similar manner.

The recent development of inhibitory-cell-type-specific transgenic mouse lines (Taniguchi et al. 2011) opens a new window for in vivo identification of inhibitory neurons. In the visual cortex, functional properties of inhibitory neurons of specific types have been examined with Ca^{2+} imaging or imaging-guided targeted recording (Kerlin et al. 2010; Ma et al. 2010; Runyan et al. 2010; Hofer et al. 2011; Atallah et al. 2012). Such studies on genetically identified inhibitory cell types, however, are lacking in the auditory cortex. Recently, extracellular unit recordings were performed from putative PV neurons, which were identified by optogenetic stimulation of PV cell population expressing channelrhodopsin-2 (Moore and Wehr 2013). However, response properties of other inhibitory cell types are unknown. Here in the mouse primary auditory cortex (A1), we performed in vivo two-photon imaging-guided targeted cell-attached and whole-cell recordings from PV and somatostatin (SOM) expressing neurons, 2 major types of cortical inhibitory neuron, and compared their frequency–intensity tonal receptive fields (TRFs) of spike output and synaptic input. Our results demonstrate that PV and SOM neurons have differential response and TRF properties, which suggest that they may engage in cortical circuits in different manners.

Materials and Methods

Animal Preparation and Auditory Cortical Mapping

All experimental procedures used in this study were approved under the Animal Care and Use Committee at the University of Southern California. The PV-ires-Cre and SOM-ires-Cre driver lines (Taniguchi et al. 2011) were crossed with Ai14 (td-Tomato) reporter mice (The Jackson laboratory). Animals were housed in a vivarium with a 12/12-h light/dark circle. Adult female mice (C57BL6 background, 2–3 months old) were sedated with chlorprothixene (0.05 mL of 4 mg/mL) and anesthetized with urethane (1.2 g/kg). Local anesthesia was applied by administrating bupivacaine subcutaneously. Experiments were carried out in

a sound-attenuation room. The left auditory cortex was exposed, and the ear canal on the same side was plugged with a piece of clay wrapped with a thin layer of cotton. The body temperature was maintained at 37.5°C by a feedback heating system (Harvard Apparatus, MA, USA). Tone pips (100-ms duration, 3-ms ramp) of various frequencies (2–32 kHz, 0.1 octave interval) and intensities (10–70 dB sound pressure level or SPL, at 10-dB interval) were generated by a custom software (LabView, National Instruments) through a 16-bit National Instruments interface, and delivered through a calibrated speaker (DT Tucker-Davis Technologies) to the contralateral ear. The 287 testing stimuli were presented in a pseudorandom sequence. Auditory cortical mapping was carried out by sequential extracellular multiunit recordings at an array of cortical sites to identify the location and frequency gradient of A1. All the experiments were carried out in the low- to middle-frequency regions (representing ~5–20 kHz) of the A1. After the recording, the mouse was perfused with 4% paraformaldehyde in phosphate-buffered saline (PBS), the brain was sectioned, and confocal fluorescence images were taken with an Olympus microscope. The labeling of cortical layers followed our previous work (Li et al. 2013).

In Vivo Two-Photon Imaging Guided Recording

In vivo two-photon imaging was performed with a custom-built imaging system. A mode-locked Ti:sapphire laser (MaiTai Broadband, Spectra-Physics) was tuned at 880 nm with the output power at 10–30 mW for layer 2/3 neurons at a depth from 150 to 300 μm. Scanning was controlled by a custom-modified scanning software (Scanimage 3.5, from Dr K. Svoboda's Laboratory, Janelia Farm, Ashburn, VA, USA). The depth of the patched cell was directly determined under imaging. For cell-attached recording, the glass electrode, with 8–10 MΩ impedance, was filled with a potassium-based intrapipette solution (in mM): 125 K-gluconate, 4 MgATP, 0.3 GTP, 10 phosphocreatine, 10 HEPES, 1 EGTA, pH 7.2, and 0.15 mM calcein (Invitrogen). The pipette tip was navigated in the cortex and patched onto a fluorescent soma as previously described (Liu et al. 2009). After confirming a successful targeting (Liu et al. 2009), a loose seal was formed (with 100–500 MΩ resistance) and maintained throughout the course of the recording. Spike responses were recorded with an Axopatch 200B amplifier (Molecular Devices). Loose-patch recording was made under voltage-clamp mode and a command potential was adjusted so that the baseline current was close to 0 pA. The recorded signal was filtered at 10 kHz and sampled at 50 kHz. For whole-cell recording, glass pipettes with larger openings (6–8 MΩ impedance) were used to form gigaohm seals after patching on a fluorescent cell body. The cell membrane was broken subsequently, and the recording was made under current-clamp mode to examine intracellular membrane potential responses. The recorded signal was filtered at 5 kHz and sampled at 20 kHz.

Tonal Receptive Field and Response Onset Latency

In cell-attached recordings, spikes could be detected without ambiguity because their amplitudes were normally higher than 100 pA, while the baseline fluctuation was <5 pA. Tone-driven spikes were counted within a 10- to 110-ms time window after the onset of tones. TRFs were reconstructed according to the array sequence. Boundaries of spike TRF were determined following previous descriptions (Sutter and Schreiner 1991; Schumacher, et al. 2011). The frequency–intensity space was first upsampled 3 times along the frequency and intensity dimensions to increase tuning resolution. A threshold at the value equal to the spontaneous spike rate plus 20% of the peak-evoked rate was then used to define significant evoked responses. Responses to frequency–intensity combinations that met this criterion were considered to fall within the TRF of the neuron, which generated the contour of the TRF (Xiong et al. 2013). Characteristic frequency (CF) was defined as the frequency (Hz) at which the lowest sound pressure level was necessary to evoke a significant excitatory response. Intensity threshold was defined as the minimum intensity to evoke a significant excitatory response. Bandwidth of TRF was determined as the total frequency range for effective tones, at the intensity level of 10 dB above the threshold (i.e., BW10), or at 60-dB SPL. To derive the bandwidth of frequency tuning curve at the half- maximum level (i.e., BW 50%), the peak firing rates at all effective tone were fitted into an envelope curve using a modified MATLAB software Envelop1.1 (developed by Lei Wang, The MathWorks), which identifies local maxima and minima in the raw dataset and then generates a smooth envelop with cubic Hermite interpolation (Sun et al. 2010, 2013). We also quantified the bandwidth of iso-intensity frequency tuning curves using σ of a Gaussian fit to the tuning curve, following Moore and Wehr (2013) study. It should be noted that the plateau shape of frequency tuning of many PV cells makes it fit poorly into a Gaussian curve (67% of PV cells displaying $R^2 < 0.3$). Following Moore and Wehr (2013) study, we excluded cells with $R^2 < 0.2$. But including all cells did not affect our conclusion. Intensity tuning was plotted for CF-tone-evoked responses as a function of evoked firing rate versus tone intensity. Intensity selectivity index (ISI) was calculated as 1 minus the ratio between the spike count at 30 dB above the preferred intensity or the highest intensity tested and that at the preferred intensity (i.e., the intensity that produced maximum spike count). Onset latency of spike response was determined from the generated peristimulus spike time histogram (PSTH) as the lag between the stimulus onset and the time point where spike rate exceeded the average baseline by 2 standard deviations of baseline fluctuations. As for membrane potential responses, response onsets were identified at the time point in the rising phase of the averaged response waveform, where the amplitude exceeded the average baseline by 2 standard deviations of baseline fluctuations.

Statistics

One-way analysis of variance (ANOVA) and post hoc test was used to compare the means of multiple groups. In the case of equal variance, post hoc Fisher's least significant difference test was applied; otherwise, Tamhane's T_2 test was applied. Kolmogorov–Smirnov test (K–S test) was applied to test the statistical difference between distributions. Bootstrap sampling (bootstrap, MATLAB, 1000 times) (Li et al. 2012) was applied to determine the statistics of ratio between spike and excitatory post-synaptic potential (EPSP) frequency range. Data were presented as mean ± SE if not otherwise specified.

Results

Tone-Evoked Spike Responses of Inhibitory Neurons In Vivo

We applied in vivo two-photon imaging-guided targeted patch recordings to determine functional properties of different types of inhibitory neurons, as well as nearby excitatory neurons in superficial layers of the primary auditory cortex in urethane-anesthetized mice. To circumvent any impacts of background noise on auditory responses, our imaging and recording system was custom-built in a sound-attenuation room, with the pumping laser and chiller isolated from the room (Fig. 1*A*). In addition, laser scanning and imaging was performed only for guiding the electrode to patch onto a cell before any auditory responses were recorded. This avoided the relatively high-level noise emitted from the scanning mirrors. Therefore, the recording system was optimized for auditory studies.

PV-Cre or SOM-Cre mice were crossed with Cre-dependent tdTomato reporter mice to label the desired subtype of inhibitory neuron with red fluorescence. Two-photon imaging-guided targeted patch recordings (Liu et al. 2009; Ma et al. 2010; Atallah et al. 2012) were made from labeled inhibitory neurons (PV or SOM) in layer 2/3 of primary auditory cortex (A1) (see Materials and Methods). Unlabeled neurons were targeted under shadow patching (Kitamura et al. 2008). The unlabeled neurons were most likely excitatory, although at a low chance (<10%), they could also be one of a variety of unlabeled inhibitory cell types. In the A1 area, PV and SOM neurons were observed across cortical layers except that PV neurons were absent in layer 1

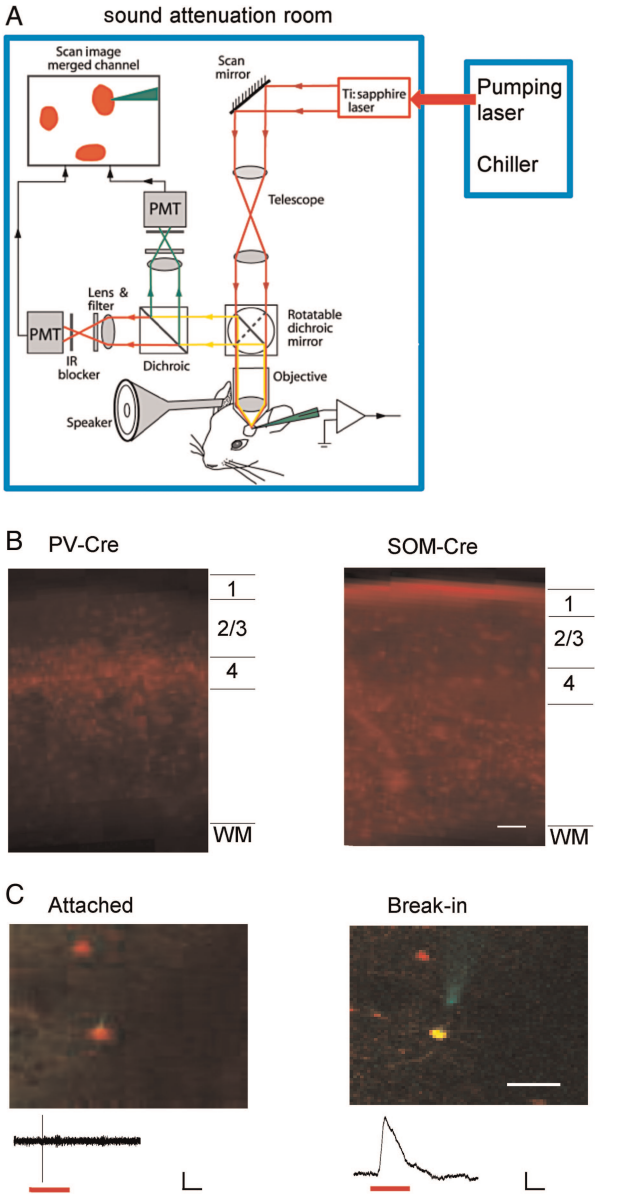

Figure 1. In vivo two-photon imaging-guided recording from auditory cortical inhibitory neurons. (*A*) The customized imaging and recording system. The pumping laser and chiller were isolated from the sound-attenuation room. Dark red lines with arrows depict the two-photon excitation pathway. Green and bright red lines depict the green and red fluorescence emission pathways, respectively. Sound stimulation was applied to the right ear through an enclosed sound delivery system. (*B*) Confocal image of a coronal section of the A1 area of a PV-Cre tdTomato and SOM-Cre tdTomato mouse, respectively, showing laminar distributions of PV and SOM neurons. Scale bar: 100 μm. (*C*) Two-photon images showing the targeted cell-attached recording from a red fluorescence-labeled neuron (left) and labeling of the cell with green fluorescence after breaking in the membrane (right). Scale bar: 33 μm. Bottom, sample-recorded spike (left) and membrane potential (right) responses, respectively. Red lines mark the tone stimulation. Scale: 30 pA (left)/7 mV (right), 50 ms.

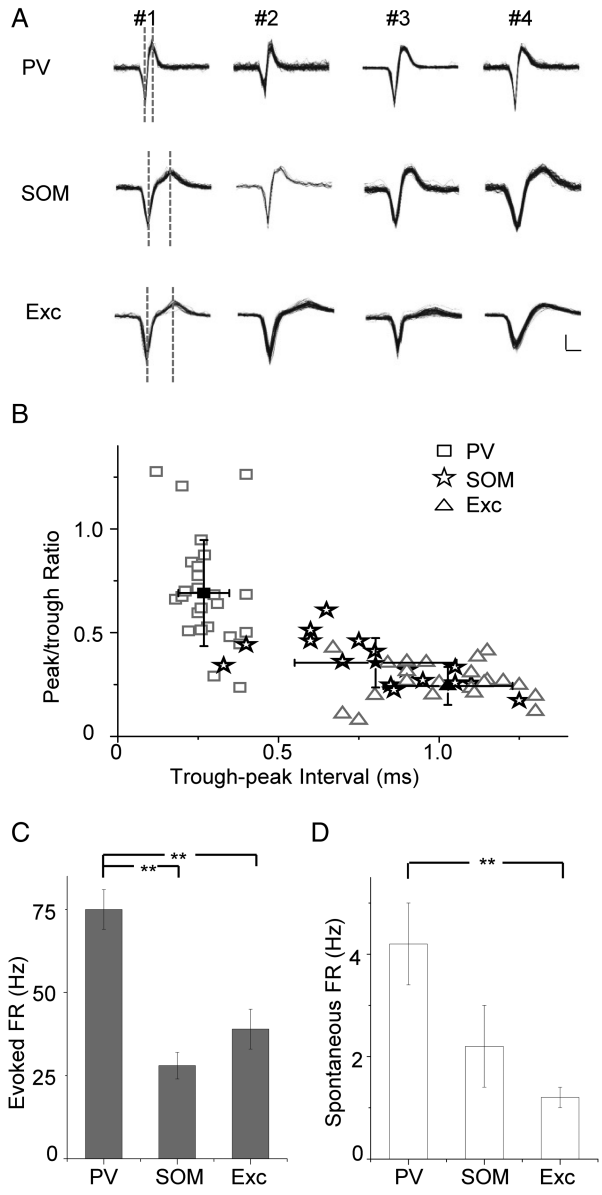

Figure 2. Spike response properties of layer 2/3 neurons in primary auditory cortex. (*A*) Spike waveforms for 4 example PV, SOM, and excitatory neurons, respectively. Black traces showing, 50 superimposed spikes. Dotted vertical lines mark the timing of the trough and peak. Scale: 40 pA, 0.5 ms. (*B*) Peak/trough amplitude ratio plotted against trough-to-peak interval (TPI) of spike waveform. Each data point is for an individual cell. Solid symbol represents mean ± SD. Peak/trough ratio: PV, 0.69 ± 0.26; SOM, 0.35 ± 0.05; Exc, 0.24 ± 0.09. Trough-peak Interval: PV, 0.27 ± 0.09 ms; SOM, 0.80 ± 0.25 ms; Exc, 1.03 ± 0.20 ms. (*C*) Average evoked firing rates for PV ($n = 27$), SOM ($n = 16$), and excitatory ($n = 22$) neurons. PV, 75 ± 6 Hz; SOM, 28 ± 4 Hz; Exc, 39 ± 6 Hz. $^{**}P < 0.01$, one-way ANOVA and post hoc test. (*D*) Average spontaneous firing rates for the 3 types of neurons. Cell numbers are the same as in (*C*). PV, 4.2 ± 0.8 Hz; SOM, 2.2 ± 0.8 Hz; Exc, 1.2 ± 0.2 Hz. $^{**}P < 0.01$, one-way ANOVA and post hoc test.

(Fig. 1*B*). We first formed a cell-attached configuration to record spikes only from the targeted cell (Fig. 1*C*, left). In a subset of experiments, gigaohm seals were achieved, and the cell membrane was subsequently broken. As a result, the cell was dialyzed with a green dye (calcein, 0.15 mM) included in the intrapipette solution. The co-localization of red and green fluorescence indicated that the desired inhibitory cell was correctly targeted (Fig. 1*C*, right).

Previous studies suggest that PV and SOM neurons may differ in their spike shapes (Tan et al. 2008; Ma et al. 2010; Levy and Reyes 2012). Similarly, we found that spike waveforms of all the recorded PV cells exhibited a trough-to-peak interval (TPI) shorter than 0.5 ms, while those of all the recorded excitatory neurons had TPIs longer than 0.5 ms (Fig. 2*A*,*B*). The majority of SOM neurons had TPIs longer than 0.5 ms, while a small percentage (13%) exhibited TPIs shorter than 0.5 ms (Fig. 2*B*). This

is consistent with previous observations that some SOM neurons had narrow spikes (Xu et al. 2006). In addition, PV neurons tended to have higher peak/trough amplitude ratios compared with the other 2 cell types (Fig. 2*B*). These data indicate that for cell-attached recording in layer 2/3, TPI of spike waveform can be used as a criterion to isolate inhibitory neurons with a reasonable accuracy. As for response level, PV neurons displayed much higher tone-evoked firing rates than SOM and excitatory cells (Fig. 2*C*). In addition, the spontaneous firing rate of PV neurons was significantly higher than excitatory cells and tended to be higher than SOM neurons (Fig. 2*D*). These data suggest that PV neurons can potentially provide stronger inhibition than SOM neurons at least in urethane anesthesia, considering that unitary synaptic connections from PV neurons are even stronger than those from SOM neurons (Levy and Reyes 2012; Pfeffer et al. 2013).

Tonal Receptive Field Properties of Inhibitory Neurons

By applying pure tones of different frequencies and intensities, we determined the TRF properties of recorded neurons. PSTHs for responses to all testing tones were plotted in the frequency–intensity space (Fig. 3*A–C*, left). As shown by 3 example cells (Fig. 3*A–C*), the PV neuron possessed apparently a larger spike TRF than the SOM and excitatory neurons. The intensity threshold, as reflected by the "tip" of the V-shaped TRF, appeared higher in the SOM than the PV and excitatory neurons (Fig. 3*A–C*, middle upper panel). To compare response temporal profiles, we generated PSTHs from spike responses to all effective tones (Fig. 3*A–C*, right upper panel). The cells all showed transient onset responses to tone stimulation. While the PV and excitatory neurons had a sharp peak in their PSTHs, the peak of the PSTH for the SOM neuron appeared relatively late and temporally broader, suggesting less precise spike times. To compare broadness of TRF, we plotted firing rates evoked by tones of different frequencies at the intensity level of 10 dB above the threshold (Fig. 3*A–C*, middle lower panel). Frequency tuning of the PV cell appeared broader than the SOM and excitatory cells, as reflected by a larger total responsive frequency range (i.e., BW10). We also examined intensity tuning by plotting firing rates evoked by CF tones at different sound intensities (Fig. 3*A–C*, right bottom panel). All the 3 example cells showed monotonically increased response levels with increasing tone intensity. Color-coded TRFs of more example cells are shown in Figure 3*D*. The trend of broader TRFs of PV neurons than SOM and excitatory cells is clear from these plots.

We recorded from 27 PV, 16 SOM, and 22 excitatory neurons. The 3 recorded cell groups did not differ in the distribution of characteristic frequencies (7–21 kHz, $P > 0.9$, K–S test between each pair of cell groups). To quantify frequency selectivity of these neurons, we measured the bandwidth of spike TRF at the intensity of 10 dB above the threshold (i.e., BW10). On average, PV neurons had TRFs twice as broad as those of SOM and excitatory neurons, while the latter 2 did not differ in their TRF bandwidths (Fig. 4*A*). In addition, we generated frequency tuning curves by fitting the frequency-dependent responses with an envelope curve (see Materials and Methods), and quantified the bandwidth of the envelope curve at the half-maximum level (i.e., BW50%) (Fig. 4*B*). Again, BW50% of PV cells was at least twice as broad as those of SOM and excitatory neurons (Fig. 4*C*). These 2 measures of frequency tuning all indicated that PV neurons were less

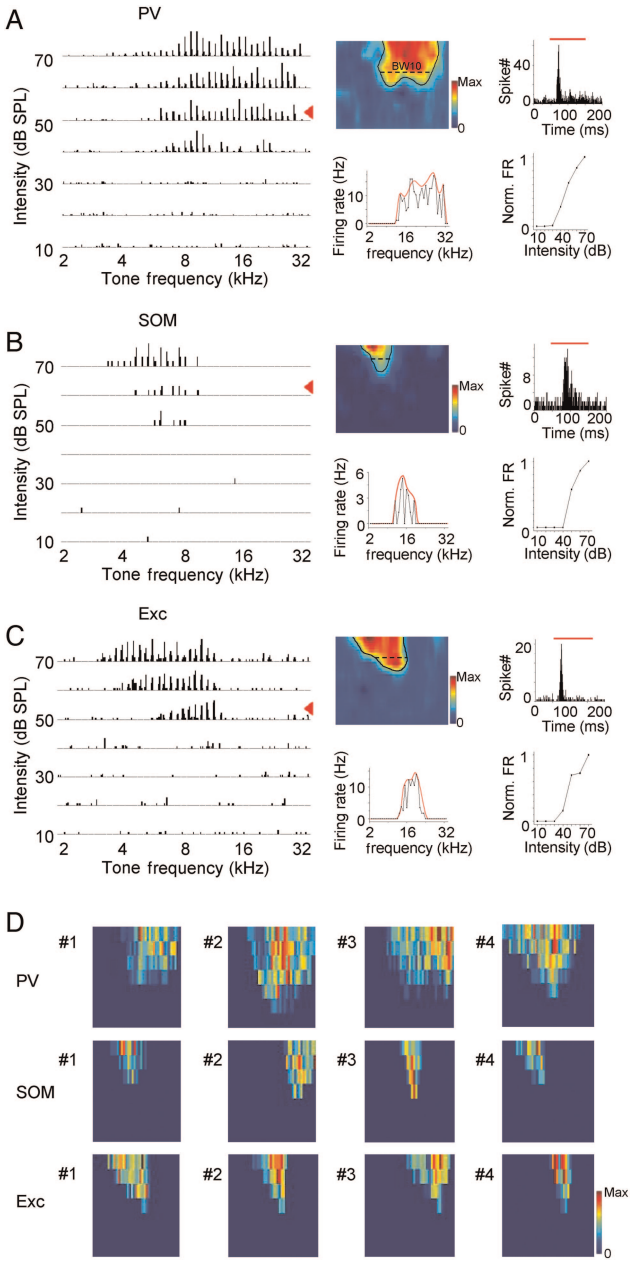

Figure 3. Tonal receptive fields of spike responses. (*A*) Left, spike TRF of an example PV neuron. Each small trace represents the PSTH for spike responses to tones at a particular frequency–intensity combination (10 trials). Middle upper panel, color map of smoothed spike TRF (see Materials and Methods). Black curve outlines the contour of the TRF. Color map depicts the average spike rates. Bandwidth at 10 dB above the intensity threshold (BW10) is marked. Color scale, 20 Hz for maximum. Middle bottom panel, evoked firing rates (black) by tones of different frequencies at the intensity level of 10 dB above the threshold (marked by the red arrowhead in the left plot). Red curve depicts the envelop for the frequency-dependent responses (see Materials and Methods), that is, frequency tuning curve. Right upper panel, PSTH generated from responses to all effective tones. Red bar marks the duration of tone stimuli. Right bottom panel, normalized firing rates evoked by CF tones at different intensities. (*B*) Spike TRF of an example SOM neuron. Data are displayed in the same manner as in (*A*). Color scale: 8.3 Hz for maximum. (*C*) Spike TRF of an example excitatory neuron. Color scale: 14 Hz for maximum. (*D*) Color maps of spike TRFs of 12 cells. Color scale: PV, 20, 27, 17, 40 Hz for maximum; SOM, 8.3, 10, 8.3, 23 Hz for maximum; Exc, 14, 12, 20, 17 Hz for maximum.

frequency-selective than SOM and excitatory neurons. Therefore, they could readily provide broadly tuned inhibition to excitatory cells. The intensity threshold of SOM neuron TRFs

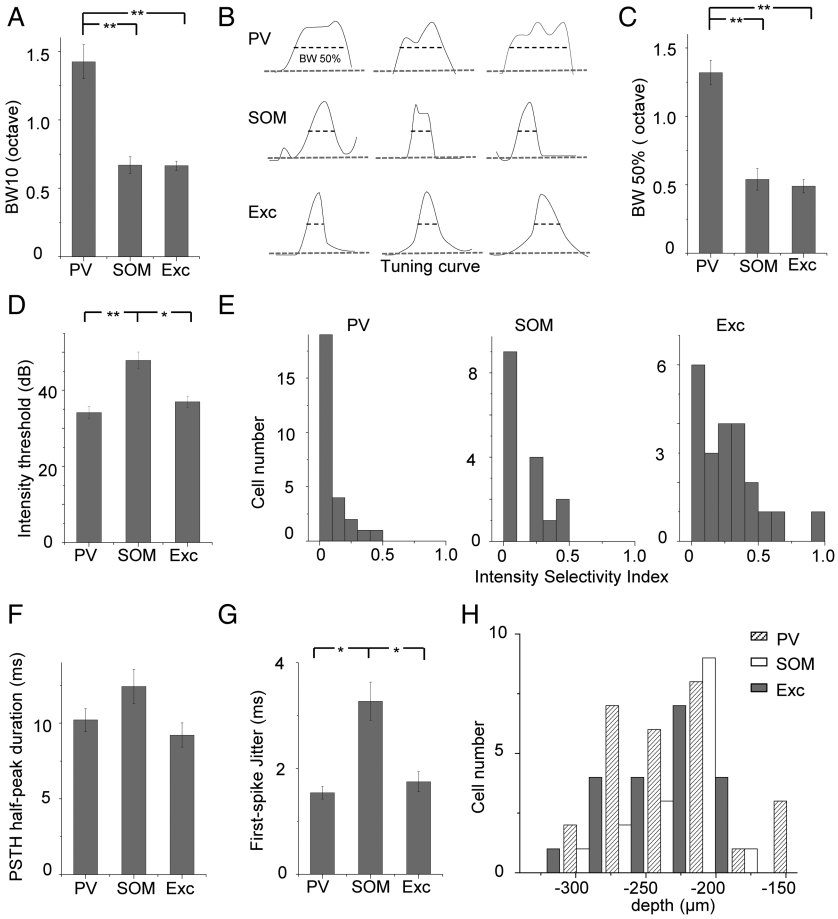

Figure 4. Summary of spike receptive field properties. (*A*) Average tuning bandwidth of TRF at 10 dB above the intensity threshold. BW10: PV, 1.43 ± 0.12 octave; SOM, 0.67 ± 0.06 octave; Exc, 0.64 ± 0.03 octave. $N = 27$ (PV), 16 (SOM) and 22 (excitatory). $^{**}P < 0.01$, ANOVA and post hoc test. (*B*) Normalized frequency tuning curves at 20 dB above the intensity threshold for 9 example cells. Gray dashed line depicts the baseline. Tuning bandwidth at the half-maximum level (i.e., BW50%) is marked. (*C*) Average BW50% at 20 dB above the intensity threshold. PV, 1.32 ± 0.09 octave; SOM, 0.54 ± 0.08 octave; Exc, 0.49 ± 0.05 octave. Cell numbers are the same as in (*A*). $^{**}P < 0.01$, ANOVA and post hoc test. (*D*) Average intensity threshold of TRF. PV, 36 ± 1.93 dB SPL; SOM, 47.86 ± 2.22 dB SPL; Exc, 40 ± 0.97 dB SPL. $^{*}P < 0.05$, $^{**}P < 0.01$, ANOVA and post hoc test. (*E*) Distribution of intensity selectivity indices in the 3 cell groups. Bin size = 0.1. (*F*) Average duration of PSTH measured at the half-maximum level for different cell groups. PV, 10.21 ± 0.75 ms; SOM, 12.43 ± 1.13 ms; Exc, 9.22 ± 0.80 ms. (*G*) Average jitter of first-spike timing calculated for responses to CF tones at 60 dB SPL. PV, 1.54 ± 0.12 ms; SOM, 3.21 ± 0.36 ms; Exc, 1.75 ± 0.19 ms. $^{*}P < 0.05$, ANOVA and post hoc test. (*H*) Distribution of cortical depths of recorded cells for different cell groups. Bin size = 30 ms.

was significantly higher than PV and excitatory neurons (Fig. 4*D*), suggesting that SOM neurons may not be able to provide inhibition under low-intensity stimuli. It is worth noting that the intensity thresholds being compared are relative rather than absolute thresholds, since, in our current experimental condition, we could not completely eliminate background noise. To compare intensity tuning, we calculated an ISI (calculated as 1 min the ratio between the spike count at 30 dB above the preferred intensity or the highest intensity tested and that at the preferred intensity) for CF-tone-evoked responses of each recorded cell. From the distributions of ISIs of 3 cell groups (Fig. 4*E*), it is clear that the majority of recorded neurons were not intensity-selective, as shown by ISIs mostly smaller than 0.5 (Wu et al. 2006), consistent with previous reports that in rodent A1 intensity-selective cells are scarce (Polley et al. 2004; Wu et al. 2006). Nevertheless, PV neurons showed significantly lower ISIs than excitatory cells ($P < 0.01$, K–S test), indicating that PV neurons were less intensity-tuned, which is consistent with the observation in a recent study (Moore and Wehr 2013). To examine temporal response properties, we measured durations of PSTHs at the half-maximum level (Fig. 4*F*). The relatively short duration of PSTHs indicated that all the 3 cell types exhibited transient onset responses to tone stimuli. In addition, we calculated jitters of response timing from repetitions of CF-tone-evoked spike responses as the standard deviation of first-spike timing. SOM neurons had significantly larger jitters of first-spike timing compared with PV and excitatory neurons (Fig. 4*G*). Consistent with their less precise spike timing, SOM neurons tended to display temporally broader PSTHs than PV and excitatory neurons (Fig. 4*F*). Finally, the 3 cell groups did not differ significantly in their distributions of cortical depths (Fig. 4*H*), indicating that the difference in frequency tuning between PV and other cell types cannot be attributed to a sampling bias of PV cells at a particular cortical depth.

Subthreshold Responses of PV and SOM Neurons

The frequency range of spike response is dependent not only on the range of synaptic input received by the neuron, but also on how efficient the synaptic input is transformed into a spike output. To understand possible mechanisms underlying the differential frequency tuning of different cell types, we carried out imaging-guided whole-cell current-clamp recordings from

genetically labeled inhibitory neurons ($n = 8$ for PV and 6 for SOM) and nearby excitatory neurons ($n = 19$) to compare their subthreshold membrane potential responses. As shown by 3 example cells (Fig. 5*A–C*) and the summarized result for responses at 60-dB SPL (Fig. 5*D*, white), the frequency range of membrane depolarization (EPSP) responses of PV cells was

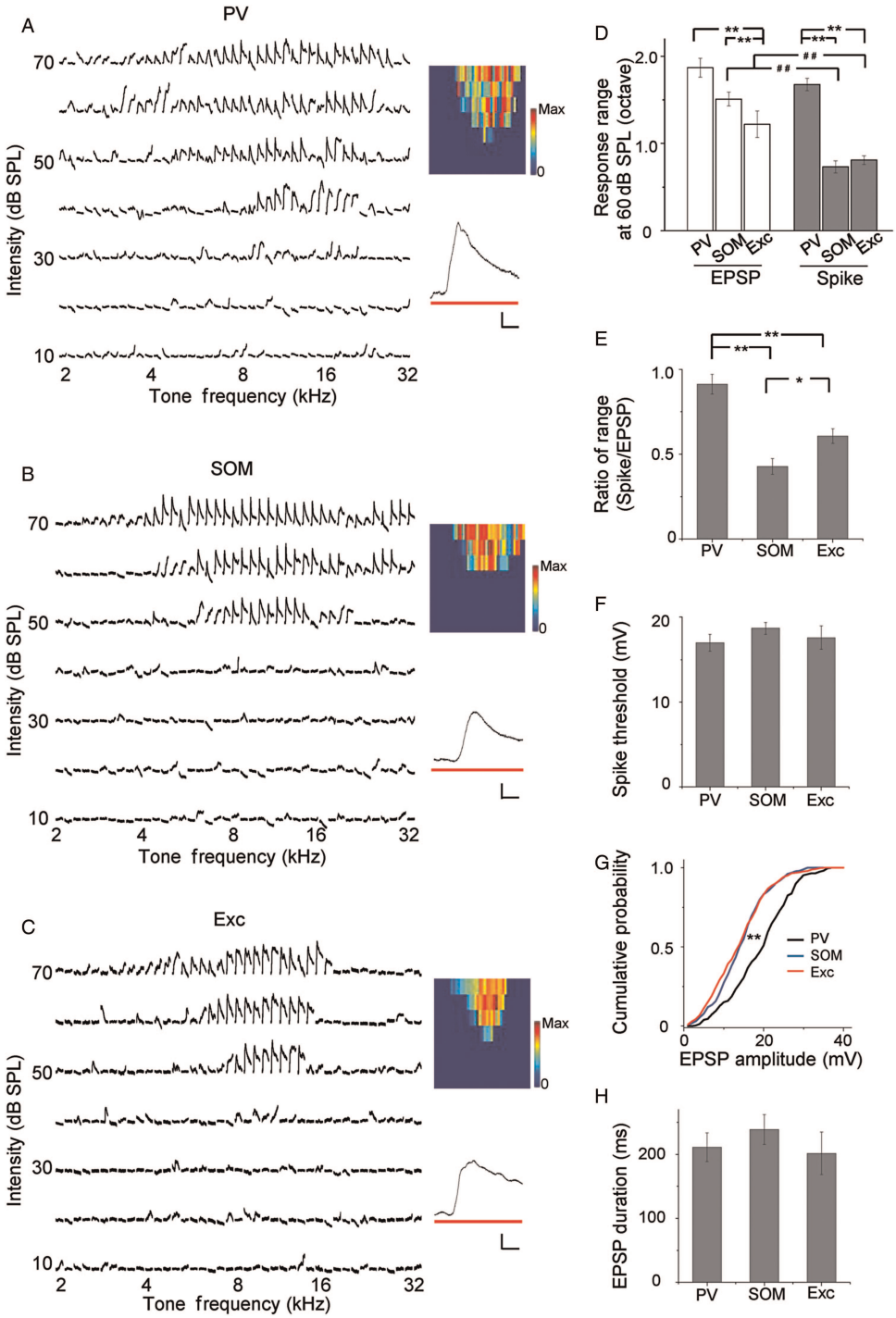

Figure 5. Tonal receptive fields of subthreshold responses. (*A*) TRF of subthreshold responses of an example PV neuron. Traces were membrane potential responses recorded in current-clamp mode with spikes filtered out. Color map depicts the peak depolarization voltages. Color scale: 30 mV for maximum. Inset, an enlarged average response trace to CF tones at 60 dB SPL. Bar denotes tone stimulation. Scale: 6 mV, 20 ms. (*B*) Subthreshold TRF of an example SOM neuron. Data are displayed in the same manner as in (*A*). Color scale: 22 mV for maximum. (*C*) Subthreshold TRF of an example excitatory neuron. Color scale: 23 mV for maximum. (*D*) Average total frequency ranges of subthreshold depolarization responses (white) and spike responses (gray) at 60 dB SPL. Subthreshold range: PV, 1.87 ± 0.11 octave ($n = 8$); SOM, 1.51 ± 0.08 octave ($n = 6$); Exc, 1.22 ± 0.15 octave ($n = 19$). Spike range: PV, 1.68 ± 0.07 octave ($n = 27$); SOM, 0.74 ± 0.07 octave ($n = 16$); Exc, 0.81 ± 0.05 octave ($n = 22$). $^{**}P < 0.01$, ANOVA and post hoc test. $\#\#P < 0.01$, *t*-test. (*E*) Ratio of spike response range over input range at 60 dB SPL for PV (0.89 ± 0.06), SOM (0.43 ± 0.05), and excitatory (0.61 ± 0.04) neurons. Bar = SD. $^{*}P < 0.05$, $^{**}P < 0.01$, bootstrapping analysis. (*F*) Average level of spike threshold relative to the resting membrane potential. PV, 17.00 ± 1.00 mV; SOM, 18.67 ± 0.67 mV; Exc, 17.60 ± 1.36 mV. (*G*) Cumulative probability of EPSP amplitudes for the 3 groups of neuron. $^{**}P < 0.01$, Kolmogorov–Smirnov test. (*H*) Average duration of EPSPs evoked by 60 dB CF tones, measured at 10% of maximum level. PV, 211.12 ± 22.28 ms; SOM, 238.89 ± 23.30 ms; Exc, 201.54 ± 33.05 ms.

significantly broader than excitatory neurons. This indicates that PV neurons recruit a broader range of excitatory inputs, which can largely account for their broader spike tuning. Interestingly, the EPSP range of SOM neurons was also significantly broader than that of excitatory neurons (Fig. 5*D*, white), although the frequency range of spike responses was not different between these 2 cell types (Fig. 5*D*, gray). The spike range was significantly smaller than the EPSP range for SOM and excitatory cells (Fig. 5*D*), as expected for an effect of spike thresholding. For PV cells, the spike range was not significantly different from the EPSPS range, although it tended to be smaller than the latter. This suggests that almost all inputs are transformed into a spike output in PV cells. Overall, the ratio of spike tuning range over input range was the highest for PV neurons, and lowest for SOM neurons (Fig. 5*E*). These results suggest that although the 2 types of inhibitory neuron both receive a broader range of excitatory input than excitatory neurons, SOM neurons are less efficient at converting the input to output, resulting in their sharp frequency tuning comparable with excitatory neurons. The high efficiency of PV neurons in converting input to output is not due to a lower spike threshold, as the 3 types of cells did not differ in the level of spike threshold (Fig. 5*F*). Notably, the amplitude of EPSPs was significantly larger in PV than SOM and excitatory neurons, as shown by the rightward shift of the cumulative distribution of EPSP amplitudes (Fig. 5*G*). On the other hand, the temporal duration of EPSP, as measured at the level of 10% of peak value, did not differ among the 3 cell groups (Fig. 5*H*). These results indicate that the broader frequency range and larger amplitudes of subthreshold responses both contribute to the broader spike tuning of PV neurons than excitatory cells.

Temporal Delay of Input and Output Responses

We further examined temporal properties of tone-evoked responses, focusing on the onset latency. In Figure 6*A*, sample spike response records to 60 dB CF tones were shown for 3 cells. These cells had similar frequency preferences (8 kHz). Notably, the evoked spiking of the PV cell was the earliest to occur, followed shortly by spiking of the excitatory neuron. The SOM neuron spiking took place much later, at about 10

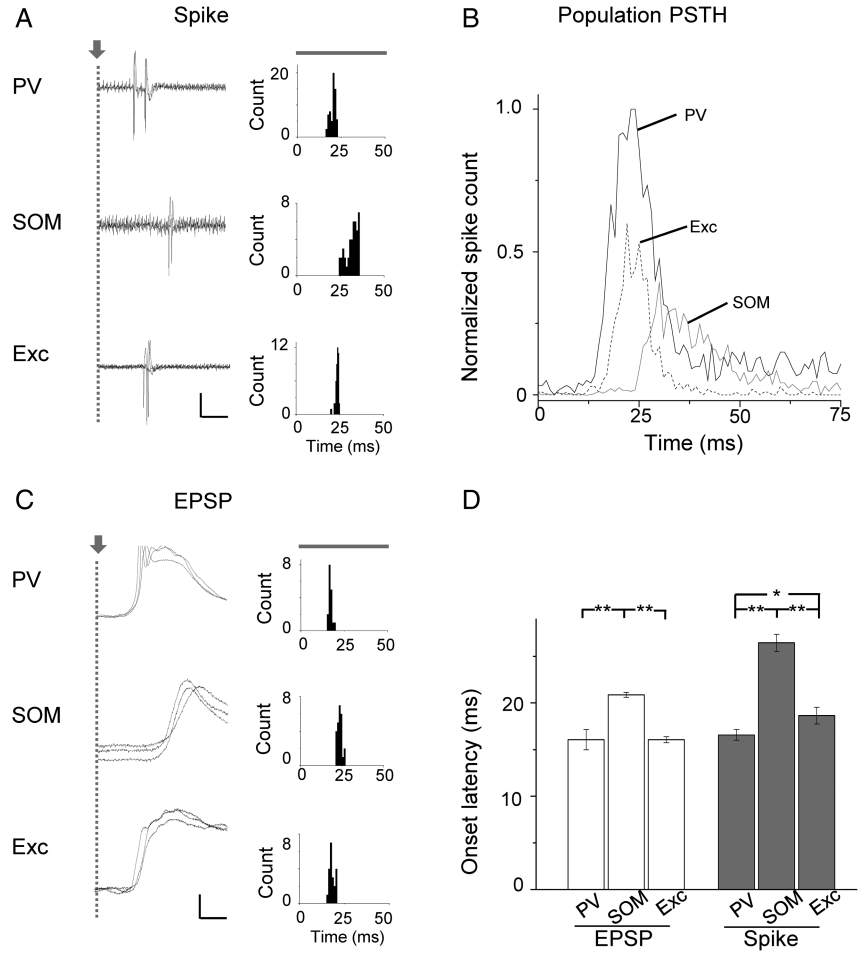

Figure 6. Temporal latencies of spike response and synaptic input. (*A*) Left, superimposed spike response traces (3 trials) to CF tones at 60 dB SPL for a PV, SOM, and excitatory neuron all preferring 8 kHz. Gray dashed line marks the tone onset. Note that 2 spikes were evoked in the PV cell, while only 1 spike was evoked in the SOM and excitatory neurons. Scale: 0.18 nA (PV), 0.07 nA (SOM), 0.2 nA (Exc), and 10 ms. Right, PSTH generated from the spike responses to CF and near CF (± 0.1 octave) tones at 60 and 50 dB SPL for the cell shown on the left. (*B*) Population PSTH generated from responses to CF and near CF tones at 60 and 50 dB SPL of all the recorded cells in each group. Bin size = 1 ms. Spike counts were averaged over trials and cell numbers and normalized to the peak value of the PV population. The tone onset is at 0 ms. Cell numbers are the same as in Figure 4*A*. (*C*) Left, recorded membrane potential responses (3 trials) for 3 example cells. Spikes are truncated. Scale: 15 mV (PV), 8 mV (SOM), 6 mV (Exc), and 10 ms. Right, distribution of onset latencies of EPSPs evoked by CF and near CF tones at 60 and 50 dB SPL. Note that a sharp peak indicates that the onset latency is relatively precise. (*D*) Average onset latencies of EPSP (white) and spike (gray) responses to CF tones at 60 dB SPL. Input: PV, 16.08 ± 1.09 ms; SOM, 20.86 ± 0.27; Exc, 16.07 ± 0.32 ms. Spike: PV, 16.59 ± 0.58 ms; SOM, 26.44 ± 0.91 ms; Exc, 18.64 ± 0.88 ms. *N* (from left to right) = 8, 19, 6; 27, 22, 16. $^{*}P < 0.05$, $^{**}P < 0.01$, ANOVA and post hoc test.

ms after the PV and excitatory neurons (Fig. 6*A*, left). We generated PSTHs from responses to tones at and near the cells' CF and at 50 and 60 dB SPL. It became clear that the onset of evoked spiking of PV and excitatory cells at the tonal receptive field "center" preceded that of SOM neurons (Fig. 6*A*, right). To reveal the overall response temporal profiles of different cell groups, we generated a "population" PSTH from spike responses of all the recorded neurons in each group to tones at and near the CF and at the intensity of 50 and 60 dB SPL (Fig. 6*B*). Such population PSTH describes the temporal profile of activation of each cell population. We found that spiking of the PV cell population slightly preceded that of the excitatory cell population. In comparison to PV and excitatory neurons, both the onset and peak of the population response of SOM neurons occurred much later, together with a lower population firing rate (Fig. 6*B*). This result indicates that PV-cell inhibition is fast enough to modulate the transient onset spiking of excitatory neurons, whereas the influence of SOM-cell inhibition is much less significant since it starts and peaks well after the excitatory cell spiking already occurs.

The delayed spiking of SOM neurons could be attributed to 2 possibilities: a delayed synaptic input and/or a prolonged integration time for spike generation (Zhou et al. 2012). To test these possibilities, we compared the onset timing of synaptic input among different cell types. As shown by 3 example cells (Fig. 6*C*, data presented in the same way as Fig. 6*A*) and the summary (Fig. 6*D*, white), synaptic input to PV cells had about the same onset delay as excitatory neurons, suggesting that PV cells, similar to excitatory neurons, receive feedforward excitatory drive. Nevertheless, PV cells spiked earlier than excitatory neurons (Fig. 6*D*, gray), likely due to a stronger excitatory drive (Fig. 5*G*). On the other hand, the onset timing of the input to SOM neurons was delayed by several milliseconds relative to PV and excitatory neurons. After another several milliseconds did the SOM neurons spike. Together, spiking of SOM neurons was delayed by about 8 ms compared with excitatory neurons, and 10 ms compared with PV neurons (Fig. 6*D*, gray). Therefore, the delayed spiking of SOM neurons could be mainly attributed to their delayed synaptic input, while a longer integration time may also contribute to their late spiking.

Discussion

With in vivo two-photon imaging targeted recordings, for the first time, we compared the functional properties of 2 major types of inhibitory neuron, the PV and SOM expressing neurons, in the auditory cortex. Our results indicate that layer 2/3 PV neurons are less selective for sound frequency compared with SOM and excitatory neurons in the same layer. Spike responses of these neurons are evoked in a PV-excitatory-SOM neuron sequence, with SOM neuron responses markedly delayed relative to PV and excitatory neurons. These results indicate that the 2 types of inhibitory neuron play differential functional roles in auditory cortical circuits.

The less-frequency and intensity selectivity property of PV neurons compared with excitatory cells is consistent with several previous reports on fast-spiking cells (Bruno and Simons 2002; Atencio and Schreiner 2008; Wu et al. 2008; Sun et al. 2013), some of which were confirmed to be inhibitory based on reconstructed morphology (Wu et al. 2008, 2011; Sun et al. 2013). The finding is also reminiscent of recent results in visual cortex that PV neurons are less orientation selective than excitatory cells (Kerlin et al. 2010; Ma et al. 2010; Hofer et al. 2011; Atallah et al. 2012, but see Runyan et al. 2010). However, a recent study also in mouse auditory cortex reported that PV neurons were as sharply tuned for frequency as excitatory cells (Moore and Wehr 2013). In that study, tuning bandwidth was compared by fitting the frequency-dependent responses with a Gaussian function. Following the method used in the Moore and Wehr study, we, however, reached the same conclusion that tuning bandwidth of PV cells was broader than SOM and excitatory cells (PV: 1.17 ± 0.10 octave; SOM: 0.52 ± 0.09 octave; Exc: 0.55 ± 0.09 octave. ANOVA and Tamhane test, $P < 0.001$ between PV and SOM; $P < 0.001$ between PV and Exc; $P > 0.05$ between SOM and Exc). The discrepancy between Moore and Wehr study and our current result may be due to different targeting methods (optogenetics aided indirect targeting vs. visually guided direct targeting). One concern about the tungsten electrode recording approach as in Moore and Wehr study is the potential contaminations from other types of units of nearby neurons. This potential problem perhaps can be prevented by coupling cell-attached loose-patch recordings with optogenetic identification, as cell-attached recording is more reliable than single-unit recording in faithfully picking up spike signals only from the patched individual neuron (Wu et al. 2008, 2011; Zhou et al. 2012). Additionally, in the Moore and Wehr study, the auditory cortex was generally recorded, while, in this study, we specifically targeted certain areas of premapped A1.

We found that the broad tuning of PV neurons can be attributed to a broad range of inputs they receive and the relatively strong excitatory drive these inputs provide. SOM neurons, although also receive a broad range of inputs, display similar frequency selectivity as excitatory neurons. This could possibly be due to a weaker net excitatory drive and/or more nonlinear firing characteristics of SOM neurons compared with PV and excitatory cells. The difference in input range between excitatory and inhibitory cells may originate in their differential local connectivity. It has been shown in layer 2/3 of mouse auditory cortex that local populations of neurons are heterogeneous in their frequency tuning (Bandyopadhyay et al. 2010; Rothschild et al. 2010). Nevertheless, the existence of subnetworks of layer 2/3 pyramidal cells with selective connectivity (i.e., connected pyramidal cells tend to receive common inputs, Yoshimura et al. 2005) would lead to relatively selective excitatory inputs to these neurons. On the other hand, connectivity between excitatory and inhibitory (in particular PV) neurons is much less selective (Yoshimura and Callaway 2005; Hofer et al. 2011; Wilson et al. 2012), which would result in a pooling of excitatory inputs with a wide range of preferred frequencies in layer 2/3 inhibitory cells. More recently, it is shown that local spatial organization of frequency tuning is much more homogenous in layer 4 than in layer 2/3 (Winkowski and Kanold 2013). This finding raises the possibility that input ranges of layer 4 excitatory and inhibitory neurons may be similar since for both types of cells the nearby neurons from which they pool inputs all have similar frequency tuning. Supporting this notion, our previous intracellular study in layer 4 of the rat auditory cortex indicates that the frequency range of synaptic input is similar between fast-spiking cells and pyramidal neurons, although the spike response range is still broader in the former cells due to a higher efficiency in converting input to spike out (Wu et al. 2008).

A visual cortical slice study has shown that the synaptic strength of PV-to-pyramidal connections is about twice as high as that of SOM-to-pyramidal connections (Pfeffer et al. 2013). Considering that PV neurons have higher evoked firing rates than SOM neurons (Fig. 2*C*), it is conceivable that PV neurons can provide much stronger inhibition to pyramidal cells than SOM neurons. It is, however, worth noting that SOM inhibition may be strongly modulated by brain and behavioral states. In the visual cortex, it is suggested that SOM neurons are more sensitive to anesthesia than PV and pyramidal neurons: sensory-evoked firing rates of SOM neurons are reduced about 10-fold in urethane anesthesia when compared with the awake running state, while the firing rates of PV neurons are not different between anesthesia and running conditions (Adesnik et al. 2012). The stronger impact of anesthesia on SOM neurons may be attributed to stronger innervations of SOM neurons by long-range corticocortical projections (top-down inputs), which are relatively inactive in anesthesia but can provide strong excitatory drive in awake states. Interestingly, in the barrel cortex, SOM neurons are spontaneously active in quiescent wakefulness, but their spiking activity is suppressed during active whisking and active touch (Gentet et al. 2012). Therefore, the modulation of sensory-evoked SOM neuron activity is complex and may depend on different cortical areas and different brain states. In this study with urethane anesthesia, SOM neurons exhibited similar evoked firing rates as excitatory neurons, as well as observable receptive fields, indicating that they do functionally connect with the cortical network. Future experiments are required to investigate whether SOM neurons in auditory cortex exhibit higher evoked firing rates in awake states than in anesthesia, and whether the increased firing rates would affect tonal receptive field properties of these cells. Nevertheless, some fundamental properties of tone-driven inputs, such as relative onset latency and frequency range, are mainly determined by ascending circuits and are likely preserved in anesthesia.

PV neurons receive their excitatory drive at the same time as excitatory neurons, and their spiking activity occurs before excitatory neurons. These results suggest that PV neurons, similar as excitatory cells, receive feedforward ascending inputs, likely from layer 4 (Barbour and Callaway 2008; Adesnik et al. 2012). Their rapid spiking enables them to provide fast feedforward inhibition to excitatory neurons to timely regulate the onset spike responses of excitatory neurons. On the other hand, SOM neurons receive delayed excitatory input, suggesting that unlike PV and excitatory neurons, SOM neurons do not receive direct ascending inputs. Instead, they are more likely driven by excitation through horizontal circuits (Adesnik et al. 2012). This notion is supported by slice recording results in visual cortex that layer 2/3 SOM neurons receive little excitation from layer 4 while PV neurons receive robust excitation from layer 4 (Adesnik et al. 2012). Consequently, spike responses of SOM neurons are significantly delayed compared with excitatory cells. The delayed feedback inhibition provided by SOM neurons is unlikely to have a significant influence on individual tone-evoked transient spike responses of excitatory cells. Nevertheless, the late inhibition may be effective in modulating spike responses to longer duration and more complex stimuli such as frequency-modulated sweeps.

PV neurons preferentially target perisomatic regions where ascending inputs are most likely located, while SOM neurons preferentially target distal dendritic domains where feedback excitatory inputs are most likely located (Di Cristo et al. 2004; Petreanu et al. 2009). These different subcellular targeting preferences led to a hypothesis that PV and SOM neurons could perform different computational functions (multiplicative vs. subtractive), which has been demonstrated in visual cortex by optogenetically manipulating PV and SOM neuron activity (Atallah et al. 2012; Lee et al. 2012; Wilson et al. 2012). In view of our current results, we suggest that PV and SOM engage in auditory cortical circuits in differential manners. PV neurons can provide broadly tuned, feedforward inhibition for a rapid control of ascending inputs to excitatory neurons through somatic integration, possibly resulting in a gain modulation of spike responses of excitatory neurons (Atallah et al. 2012; Wilson et al. 2012). SOM neurons, on the other hand, provide delayed and selective inhibition to modulate the feedback excitatory inputs on the distal dendrites of excitatory neurons in a more specific manner.

Funding

This work was supported by grants from the US National Institutes of Health (DC008983 to L.I.Z. and EY019049 to H.W.T.), and the David and Lucile Packard Foundation (Packard Fellowships for Science and Engineering) to L.I.Z. W.Y. was supported by grants from the National Natural Science Foundation of China (30973301 and 81271080).

Notes

Conflict of Interest: None declared.

References

Adesnik H, Bruns W, Taniguchi H, Huang ZJ, Scanziani M. 2012. A neural circuit for spatial summation in visual cortex. Nature. 490:226–231.

Andermann ML, Ritt J, Neimark MA, Moore CI. 2004. Neural correlates of vibrissa resonance; band-pass and somatotopic representation of high frequency stimuli. Neuron. 42:451–463.

Atallah BV, Bruns W, Carandini M, Scanziani M. 2012. Parvalbumin-expressing interneurons linearly transform cortical responses to visual stimuli. Neuron. 73:159–170.

Atencio CA, Schreiner CE. 2008. Spectrotemporal processing differences between auditory cortical fast-spiking and regular-spiking neurons. J Neurosci. 28:3897–3910.

Bandyopadhyay S, Shamma SA, Kanold PO. 2010. Dichotomy of functional organization in the mouse auditory cortex. Nat Neurosci. 13:361–368.

Barbour DL, Callaway EM. 2008. Excitatory local connections of superficial neurons in rat auditory cortex. J Neurosci. 28:11174–11185.

Barthó P, Hirase H, Monconduit L, Zugaro M, Harris KD, Buzsáki G. 2004. Characterization of neocortical principal cells and interneurons by network interactions and extracellular features. J Neurophysiol. 92:600–608.

Bruno RM, Simons DJ. 2002. Feedforward mechanisms of excitatory and inhibitory cortical receptive fields. J Neurosci. 22:10966–10975.

Callaway EM. 1998. Local circuits in primary visual cortex of the macaque monkey. Annu Rev Neurosci. 21:47–74.

Di Cristo G, Wu C, Chattopadhyaya B, Ango F, Knott G, Welker E, Svoboda K, Huang ZJ. 2004. Subcellular domain-restricted GABAergic innervations in primary visual cortex in the absence of sensory and thalamic inputs. Nat Neurosci. 7:1184–1186.

Douglas RJ, Martin KA. 2004. Neuronal circuits of the neocortex. Annu Rev Neurosci. 27:419–451.

Gentet LJ, Kremer Y, Taniguchi H, Huang ZJ, Staiger JF, Petersen CC. 2012. Unique functional properties of somatostatin-expressing GABAergic neurons in mouse barrel cortex. Nat Neurosci. 15:607–612.

Gray CM, McCormick DA. 1996. Chattering cells: superficial pyramidal neurons contributing to the generation of synchronous oscillations in the visual cortex. Science. 274:109–113.
Hofer SB, Ko H, Pichler B, Vogelstein J, Ros H, Zeng H, Lein E, Lesica NA, Mrsic-Flogel TD. 2011. Differential connectivity and response dynamics of excitatory and inhibitory neurons in visual cortex. Nat Neurosci. 14:1045–1052.
Kawaguchi Y, Kubota Y. 1997. GABAergic cell subtypes and their synaptic connections in rat frontal cortex. Cereb Cortex. 7:476–486.
Kerlin AM, Andermann ML, Berezovskii VK, Reid RC. 2010. Broadly tuned response properties of diverse inhibitory neuron subtypes in mouse visual cortex. Neuron. 67:858–871.
Kitamura K, Judkewitz B, Kano M, Denk W, Häusser M. 2008. Targeted patch-clamp recordings and single-cell electroporation of unlabeled neurons in vivo. Nat Methods. 5:61–67.
Lee SH, Kwan AC, Zhang S, Phoumthipphavong V, Flannery JG, Masmanidis SC, Taniguchi H, Huang ZJ, Zhang F, Boyden ES et al. 2012. Activation of specific interneurons improves V1 feature selectivity and visual perception. Nature. 488:379–383.
Levy RB, Reyes AD. 2012. Spatial profile of excitatory and inhibitory synaptic connectivity in mouse primary auditory cortex. J Neurosci. 32:5609–5619.
Li LY, Li YT, Zhou M, Tao HW, Zhang LI. 2013. Intracortical multiplication of thalamocortical signals in mouse auditory cortex. Nat Neurosci. 16:1179–1181.
Li YT, Ma WP, Li LY, Ibrahim LA, Wang SZ, Tao HW. 2012. Broadening of inhibitory tuning underlies contrast-dependent sharpening of orientation selectivity in mouse visual cortex. J Neurosci. 32:16466–16477.
Liu BH, Li P, Li YT, Sun YJ, Yanagawa Y, Obata K, Zhang LI, Tao HW. 2009. Visual receptive field structure of cortical inhibitory neurons revealed by two-photon imaging guided recording. J Neurosci. 29:10520–10532.
Ma WP, Liu BH, Li YT, Huang ZJ, Zhang LI, Tao HW. 2010. Visual representations by cortical somatostatin inhibitory neurons—selective but with weak and delayed responses. J Neurosci. 30:14371–14379.
Markram H, Toledo-Rodriguez M, Wang Y, Gupta A, Silberberg G, Wu C. 2004. Interneurons of the neocortical inhibitory system. Nat Rev Neurosci. 5:793–807.
Moore AK, Wehr M. 2013. Parvalbumin-expressing inhibitory interneurons in auditory cortex are well-tuned for frequency. J Neurosci. 33:13713–13723.
Petreanu L, Mao T, Sternson SM, Svoboda K. 2009. The subcellular organization of neocortical excitatory connections. Nature. 457:1142–1145.
Pfeffer CK, Xue M, He M, Huang ZJ, Scanziani M. 2013. Inhibition of inhibition in visual cortex: the logic of connections between molecularly distinct interneurons. Nat Neurosci. 16:1068–1076.
Polley DB, Heiser MA, Blake DT, Schreiner CE, Merzenich MM. 2004. Associative learning shapes the neural code for stimulus magnitude in primary auditory cortex. Proc Natl Acad Sci USA. 101:16351–16356.
Razak KA, Fuzessery ZM. 2010. GABA shapes a systematic map of binaural sensitivity in the auditory cortex. J Neurophysiol. 104:517–528.
Rothschild G, Nelken I, Mizrahi A. 2010. Functional organization and population dynamics in the mouse primary auditory cortex. Nat Neurosci. 13:353–360.
Runyan CA, Schummers J, Van Wart A, Kuhlman SJ, Wilson NR, Huang ZJ, Sur M. 2010. Response features of parvalbumin-expressing interneurons suggest precise roles for subtypes of inhibition in visual cortex. Neuron. 67:847–857.
Sadagopan S, Wang X. 2010. Contribution of inhibition to stimulus selectivity in primary auditory cortex of awake primates. J Neurosci. 30:7314–7325.
Schumacher JW, Schneider DM, Woolley SM. 2011. Anesthetic state modulates excitability but not spectral tuning or neural discrimination in single auditory midbrain neurons. J Neurophysiol. 106:500–514.
Sun YJ, Kim YJ, Ibrahim LA, Tao HW, Zhang LI. 2013. Synaptic mechanisms underlying functional dichotomy between intrinsic-bursting and regular-spiking neurons in auditory cortical layer 5. J Neurosci. 33:5326–5339.
Sun YJ, Wu GK, Liu BH, Li P, Zhou M, Xiao Z, Tao HW, Zhang LI. 2010. Fine-tuning of pre-balanced excitation and inhibition during auditory cortical development. Nature. 465:927–931.
Sutter ML, Schreiner CE. 1991. Physiology and topography of neurons with multipeaked tuning curves in cat primary auditory cortex. J Neurophysiol. 65:1207–1226.
Tan AY, Atencio CA, Polley DB, Merzenich MM, Schreiner CE. 2007. Unbalanced synaptic inhibition can create intensity-tuned auditory cortex neurons. Neuroscience. 146:449–462.
Tan AY, Zhang LI, Merzenich MM, Schreiner CE. 2004. Tone-evoked excitatory and inhibitory synaptic conductances of primary auditory cortex neurons. J Neurophysiol. 92:630–643.
Tan Z, Hu H, Huang ZJ, Agmon A. 2008. Robust but delayed thalamocortical activation of dendritic-targeting inhibitory interneurons. Proc Natl Acad Sci USA. 105:2187–2192.
Taniguchi H, He M, Wu P, Kim S, Paik R, Sugino K, Kvitsiani D, Fu Y, Lu J, Lin Y et al. 2011. A resource of Cre driver lines for genetic targeting of GABAergic neurons in cerebral cortex. Neuron. 71: 995–1013.
Wehr M, Zador AM. 2003. Balanced inhibition underlies tuning and sharpens spike timing in auditory cortex. Nature. 426:442–446.
Wilson NR, Runyan CA, Wang FL, Sur M. 2012. Division and subtraction by distinct cortical inhibitory networks in vivo. Nature. 488:343–348.
Winkowski DE, Kanold PO. 2013. Laminar transformation of frequency organization in auditory cortex. J Neurosci. 33:1498–1508.
Wu GK, Arbuckle R, Liu BH, Tao HW, Zhang LI. 2008. Lateral sharpening of cortical frequency tuning by approximately balanced inhibition. Neuron. 58:132–143.
Wu GK, Li P, Tao HW, Zhang LI. 2006. Nonmonotonic synaptic excitation and imbalanced inhibition underlying cortical intensity tuning. Neuron. 52:705–715.
Wu GK, Tao HW, Zhang LI. 2011. From elementary synaptic circuits to information processing in primary auditory cortex. Neurosci Biobehav Rev. 35:2094–2104.
Xiong XR, Liang F, Li H, Mesik L, Zhang KK, Polley DB, Tao HW, Xiao Z, Zhang LI. 2013. Interaural level difference-dependent gain control and synaptic scaling underlying binaural computation. Neuron. 79:738–753.
Xu X, Roby KD, Callaway EM. 2006. Mouse cortical inhibitory neuron type that coexpresses somatostatin and calretinin. J Comp Neurol. 499:144–160.
Yoshimura Y, Callaway EM. 2005. Fine-scale specificity of cortical networks depends on inhibitory cell type and connectivity. Nat Neurosci. 8:1552–1559.
Yoshimura Y, Dantzker JL, Callaway EM. 2005. Excitatory cortical neurons form fine-scale functional networks. Nature. 433:868–873.
Zhang LI, Tan AY, Schreiner CE, Merzenich MM. 2003. Topography and synaptic shaping of direction selectivity in primary auditory cortex. Nature. 424:201–205.
Zhou Y, Mesik L, Sun YJ, Liang F, Xiao Z, Tao HW, Zhang LI. 2012. Generation of spike latency tuning by thalamocortical circuits in auditory cortex. J Neurosci. 32:9969–9980.